Int J Adv Manuf Technol (2016) 85:2873–2885
DOI 10.1007/s00170-015-8120-0

ORIGINAL ARTICLE

Eye-in-hand vision-based robotic bin-picking with active laser projection

Wen-Chung Chang[1] · **Chia-Hung Wu**[2]

Received: 7 July 2015 / Accepted: 12 November 2015 / Published online: 27 November 2015

Abstract In this paper, an eye-in-hand vision-based robotic bin-picking system is proposed. The system can identify the pose of a plumbing part from a pile and grip it correctly. A monocular eye-in-hand camera and a laser projector are employed to reconstruct the 3-D point cloud of plumbing parts stacked together. The projection direction of the laser line projector is controlled to change in order to scan the pile of objects while the camera is observing. 3-D points can then be determined by the a priori known geometry between the camera and the laser line projector. To estimate the pose of an object, the iterative closest point (ICP) is employed to match the point clouds of the object and the model. The transformation between the object and the model can thus be determined. A computed closer point (CCP) approach is proposed to estimate the pose of an object since the deviation from the object to the model is initially large in nature. The proposed CCP approach combining with the ICP algorithm can improve the success rate and accuracy of point cloud matching. The proposed system has been validated by experiments with potential applications in production lines.

Keywords CCP · Eye-in-hand · ICP · Laser projection · Random bin-picking · Robotic manipulator

✉ Wen-Chung Chang
wchang@ntut.edu.tw

[1] Department of Electrical Engineering (DEE2125), National Taipei University of Technology, Taipei 106, Taiwan

[2] Department of Electrical Engineering, National Taipei University of Technology, Taipei 106, Taiwan

1 Introduction

Industrial automation technologies have been developed continuously to improve effectiveness and efficiency of manufacturing. Repeated and monotonous manual work is gradually replaced by automated systems [3]. In production lines, bin-picking work is almost executed by human operators. For increasing performance of the work, automated bin-picking systems become popular alternatives to replace manual work. Key problems of bin-picking systems include observing objects and computing poses of objects. According to different production lines, a variety of distinctions can be seen in geometric shapes, colors, and surfaces of objects to be processed. This causes the design of bin-picking a challenging and complex issue.

To observe objects and reconstruct 3-D data, some non-contact sensors can be considered to measure objects. Camera is a convenient sensor which can be employed to measure 3-D data. For the purpose of reconstructing, a solution is to use cameras with a projector [13]. In particular, a coded structured light is projected onto objects by the projector and a camera captures variations of structured light in images. By analyzing variations of structured light, 3-D data can be reconstructed. Many studies have been focused on multiple kinds of coded structured light. Structured light can be designed in gray level or color space. General designs are binary codes [17] or phase shifting [11, 20, 21]. According to the depth of an object, one can determine 3-D information by the variation of pixel intensity. Another way is to design coded structured light in RGB color space. M-array is such kind of coded color structured light [10]. In color space, image processing can be faster and more accurate because recognition rate is higher than the case in gray level. In addition to the above-described ways, laser projectors can also be employed [14, 22]. A laser projector can project a single

color structured light such as line, cross, or grids. This kind of laser projector can be used to scan objects [15] and then reconstruct 3-D data with cameras [4, 8, 25]. More recently, some 3-D sensors are also employed in industry. For example, a range camera can be used to detect 3-D data of targets directly [12].

To estimate the pose of an object, many approaches have been proposed. Identifying and matching structures and shapes is a solution to determine the poses of objects. Xu et al. [23] proposed a 3-D pose estimation method using convex hull. In this way, one can design corresponding conditions to estimate the pose of a specific object fastly. Another way is matching an object and a model by using 3-D data. Point cloud, a set of points, is often used to determine the pose of an object. The iterative closest point (ICP) algorithm [2] is an illustrious algorithm that can be used to match two point clouds and then compute the transformation matrix between them. The ICP algorithm employs closest point matching method to match points from reconstructed data point cloud to model point cloud. By applying this relation, a transformation between two point clouds can be determined after a number of iterations. Because some closest points are not corresponding points in general, the result of computation may be inaccurate. If the deviation of a data point cloud from a model point cloud is large, the result of matching these two point clouds and the transformation between them cannot be successfully completed in most cases. Some studies have been focused on improving the ICP algorithm [5, 6, 24].

A typical bin-picking system includes target detection, pose estimation, and gripping manipulation. Rodrigues et al. [18] proposed a bin-picking system that employs a single camera to measure objects in 2-D images, and the poses of objects can be estimated by 2-D data. Some systems employ 3-D cameras [16] or a camera with a laser projector [1] to scan objects for a manipulator to pick up an object from a bin. Based on 3-D data, the pose of a target can be estimated by using 3-D templates [19]. In this research, the proposed bin-picking system employs an active laser projector to reconstruct 3-D point cloud for pose estimation. The 3-D point cloud will be segmented by using a segmentation approach. For the purpose of determining the pose of an object, a computed closer point (CCP) approach is proposed that is based on object geometry. This approach can be used to estimate the pose of an object roughly to reduce the difference between the poses of an object and its model. After executing the CCP approach, the ICP algorithm is employed to estimate the pose of the object accurately. Then, the system enables a manipulator to grip an object repeatedly based on the pose estimation result. The paper is organized as follows. Firstly, system description and problem formulation are given in Section 2. The 3-D point cloud reconstruction approach by using active laser projection and an eye-in-hand camera is presented in Section 3. The CCP approach is explained in Section 4. Experimental results are presented in Section 5. Finally, conclusion is given in Section 6.

2 The system

2.1 System description

A robotic bin-picking system must be able to handle two main procedures, object detection and pose estimation. When a pile of objects is placed in the workspace, the system must be able to detect a grabbable object and determine its pose. Thus, the system is able to compute the corresponding command to drive a manipulator to grab the object. The proposed system consists of a single camera with an active laser line projector for 3-D reconstruction, and a robotic manipulator with a gripper for grabbing objects. The target is a pile of plumbing parts. The system configuration is shown in Fig. 1. The system employs 3-D point cloud to identify a single plumbing part from a pile and determine its pose.

For the purpose of reconstructing a 3-D data point cloud of objects, a camera with an active laser line projector is employed. When the laser line projector projects a line to the objects, the camera captures images and then a point cloud can be reconstructed by applying the geometric relation between the camera and the laser line projector. To measure integrated data point cloud, a motor driving the

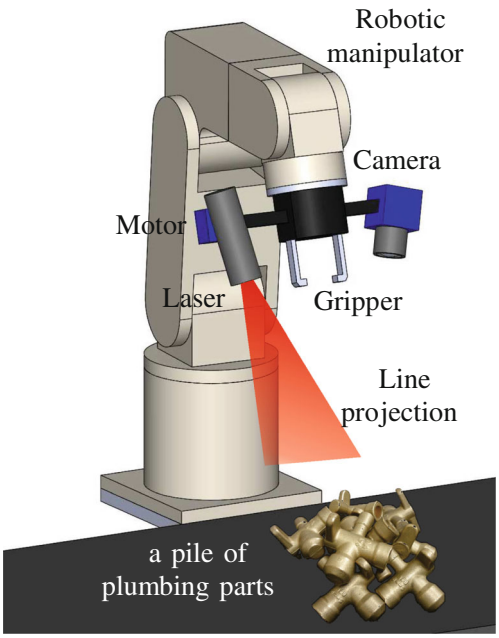

Fig. 1 The system configuration

laser line projector rotates for direction change. The reconstructed point cloud contains multiple objects in a pile. To identify a single object from the point cloud, a segmentation approach must be employed to segment the top object as illustrated in Fig. 2a. In this paper, the ICP algorithm is employed to determine the transformation between two point clouds. The pose of the top object is determined based on the transformation from the model point cloud to the data point cloud. Because the transformation may be stuck in a local minimum by iterations of the ICP algorithm when the deviation from the data point cloud to the model point cloud is large. The proposed CCP approach is used to resolve this problem that estimates the pose roughly by the geometry of the data point cloud before employing the ICP algorithm. This way the success rate of two point clouds matching can be effectively improved since the poses between two point clouds are large in nature as shown in Fig. 2b. Figure 3 illustrates the process of the proposed system.

2.2 Problem formulation

2.2.1 Target pose estimation

For the purpose of driving the manipulator to grab an object correctly, the pose of an object must be determined. One can estimate the object pose based on its 3-D model known a priori. The pose of the model in the base frame $\{B\}$ is written as

$$ {}^{B}\boldsymbol{x}_{M} = \begin{bmatrix} \boldsymbol{p}_{M} \\ \boldsymbol{\theta}_{M} \end{bmatrix} \tag{1} $$

where $\boldsymbol{p}$ and $\boldsymbol{\theta}$ denote the position and the orientation of the model, respectively. Based on the pose ${}^{0}\boldsymbol{x}_{M}$, the transformation matrix describing the model frame $\{M\}$ relative to the base frame $\{B\}$ can be determined as follows:

$$ {}^{B}_{M}\boldsymbol{T} = \begin{bmatrix} {}^{B}_{M}\boldsymbol{R}(\boldsymbol{\theta}_{M}) & {}^{B}\boldsymbol{p}_{M} \\ \boldsymbol{0}_{1\times 3} & 1 \end{bmatrix}. \tag{2} $$

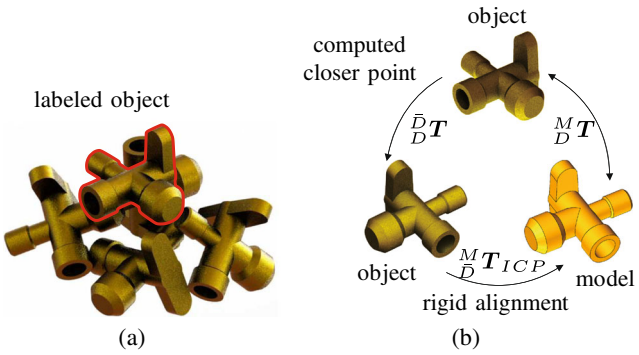

Fig. 2 **a**, **b** Schematic diagram of point cloud segmentation and matching

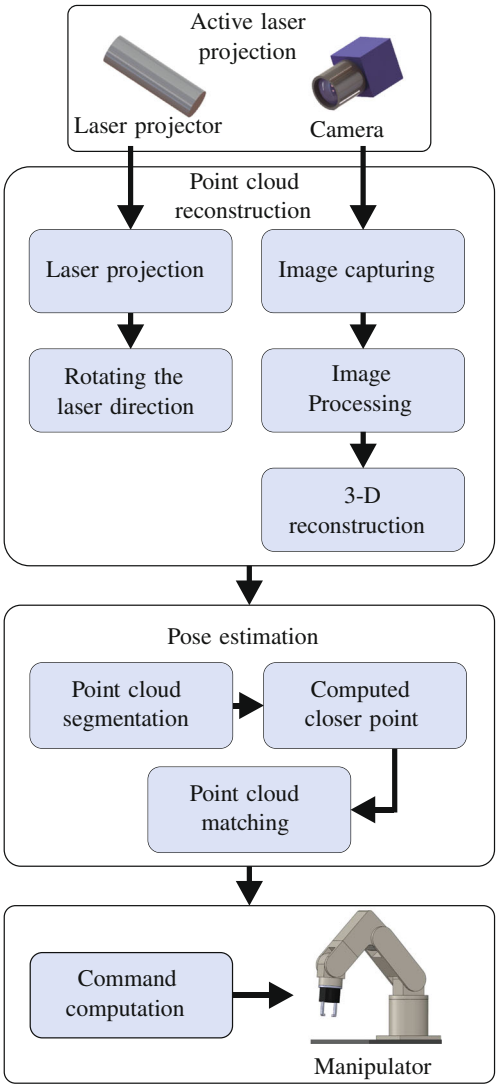

Fig. 3 The diagram of the proposed system

According to ${}^{B}_{M}\boldsymbol{T}$, if the transformation matrix ${}^{M}_{D}\boldsymbol{T}$ from the object frame $\{D\}$ to the model frame $\{M\}$ can be determined, the transformation matrix ${}^{B}_{D}\boldsymbol{T}$ from the object frame $\{D\}$ to the base frame $\{B\}$ can then be determined as follows:

$$ {}^{B}_{D}\boldsymbol{T} = {}^{B}_{M}\boldsymbol{T}\,{}^{M}_{D}\boldsymbol{T} \tag{3} $$

where

$$ {}^{M}_{D}\boldsymbol{T} = \begin{bmatrix} {}^{M}_{D}\boldsymbol{R}(\boldsymbol{\theta}_{D}) & {}^{M}\boldsymbol{p}_{D} \\ \boldsymbol{0}_{1\times 3} & 1 \end{bmatrix}. \tag{4} $$

Because the object is placed randomly, the reconstructed 3-D data pose $\begin{bmatrix} \boldsymbol{p}_{D}^{T} & \boldsymbol{\theta}_{D}^{T} \end{bmatrix}^{T}$ is unknown. To grab the object precisely, the pose must be estimated correctly. If the 3-D data of the model and the object are available in the form of 3-D point cloud, the ICP algorithm can be employed to match two point clouds and estimate the transformation matrix from the object to the model. But the matching may

fail if the values of ${}^{M}\boldsymbol{p}_D$ and $\boldsymbol{\theta}_D$ are large which is generally true in typical cases. To solve this problem, the CCP (computed closer point) approach is proposed to estimate the pose of the object to reduce its deviation from the pose of the model.

$$ {}^{\bar{D}}_{D}\boldsymbol{T} = \begin{bmatrix} {}^{\bar{D}}_{D}\boldsymbol{R}(\boldsymbol{\theta}_D) & {}^{\bar{D}}\boldsymbol{p}_D \\ \boldsymbol{0}_{1\times 3} & 1 \end{bmatrix} \tag{5} $$

The original pose of the object is designed to be transformed to a pose close to the model where $\{\bar{D}\}$ denotes the closer object frame. The transformed object data can thus be employed in iterations of the ICP to compute accurate transformation matrix ${}^{M}_{\bar{D}}\boldsymbol{T}_{\mathrm{ICP}}$ from the closer object to the model. Then, the system can determine the transformation from the model frame $\{M\}$ to the object frame $\{D\}$ by Eq. (5) and ${}^{M}_{\bar{D}}\boldsymbol{T}_{\mathrm{ICP}}$ as follows:

$$ {}^{M}_{D}\boldsymbol{T} = {}^{M}_{\bar{D}}\boldsymbol{T}_{\mathrm{ICP}}\,{}^{\bar{D}}_{D}\boldsymbol{T}. \tag{6} $$

Thus, the pose of the object can be determined by Eq. (3).

2.2.2 Calibration of reconstruction system

The proposed system employs a laser line projector and a CCD camera to measure and reconstruct 3-D points. The laser line projected along the optical axis is extended to a plane. If the pose of the laser line projector is determined, 3-D points $\boldsymbol{g}_{\mathrm{i}}$ can be reconstructed based on the observed images of the camera and the geometry between the camera and the laser line projector as follows:

$$ \boldsymbol{g}_i = f_r\left({}^{C}_{L}\boldsymbol{T}, \boldsymbol{r}_{\mathrm{i}}\right) \tag{7} $$

where ${}^{C}_{L}\boldsymbol{T}$ denotes the transformation relating the laser line projector frame $\{L\}$ to the camera frame $\{C\}$, and $\boldsymbol{r}_{\mathrm{i}}$ is the position in the image. The calibration problem is to compute the laser projector pose in the camera frame.

3 Point cloud reconstruction with active laser projection

The proposed system employs 3-D point clouds to estimate object poses. Thus, the point clouds of model and real objects are essential to resolving the estimation problem. The model point cloud can be created off-line, but the data point cloud must be reconstructed by an appropriate sensor in real time. Specifically, a single camera and an active laser line projector are employed to scan objects. The laser line projector projects a red straight line and is rotated to change the direction of projection by an AI motor. The advantages of employing a laser line projector are that the color of the projection can be easily identified and the density of point cloud is high. Denser data allows to estimate the pose of an object correctly. Meanwhile, the cost of laser projectors is lower than LED projectors or other 3-D sensors. Moreover, a variety of the structured light patterns can be considered. Compared with LED projectors, laser projectors allow clearer projection in a larger workspace. Figure 4 shows the configuration of the reconstruction system.

3.1 Active laser projection

The reconstruction is based on the geometry of the laser line projector and the camera. When the laser line projector projects a line pattern, the line will be extended to a plane along the direction of the optical axis. According to the plane and images, real 3-D points can be determined. The transformation matrix from the camera frame $\{C\}$ to the laser line projector frame $\{L\}$ is

$$ {}^{C}_{L}\boldsymbol{T} = \begin{bmatrix} {}^{C}_{L}\boldsymbol{R} & {}^{C}\boldsymbol{p}_{\mathrm{LORG}} \\ \boldsymbol{0}_{1\times 3} & 1 \end{bmatrix}. \tag{8} $$

where ${}^{C}_{L}\boldsymbol{R}$ denotes the rotation matrix relating $\{L\}$ to $\{C\}$ and ${}^{C}\boldsymbol{p}_{\mathrm{LORG}}$ denotes the vector that locates the origin of the frame $\{L\}$. Because the laser projector projects a line pattern along z-axis,the projected pattern can be considered as a laser plane. The normal vector of the plane and x-axis of the laser projector frame are assumed parallel. The normal vector can be transformed from the laser projector frame to the camera frame as follows:

$$ {}^{C}\boldsymbol{n} = {}^{C}_{L}\boldsymbol{R}\,{}^{L}\boldsymbol{n} \tag{9} $$

where ${}^{C}\boldsymbol{n} = \begin{bmatrix} {}^{C}n_x & {}^{C}n_y & {}^{C}n_z \end{bmatrix}^T$ is the normal vector of the laser plane in the camera frame $\{C\}$ and ${}^{L}\boldsymbol{n}$ is the unit vector along x-axis of the laser projector frame $\{L\}$. The

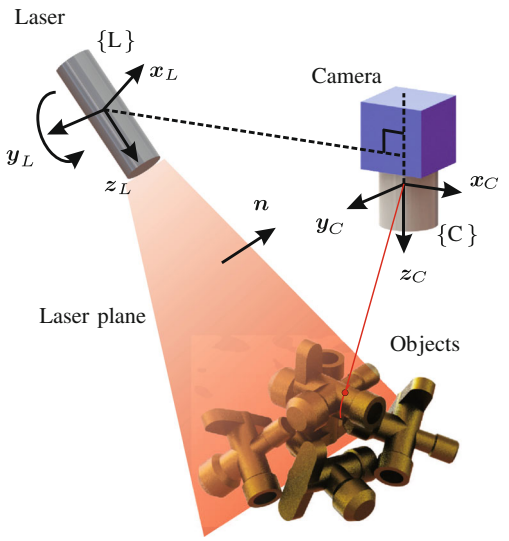

Fig. 4 The configuration of the reconstruction system

equation of laser plane in the camera frame can be described as follows:

$$^{C}n_x x +^{C} n_y y +^{C} n_z z -^{C} \boldsymbol{n} \cdot^{C} \boldsymbol{p}_{\mathrm{LORG}} = 0 \tag{10}$$

In the proposed system, the laser projector is assumed to be rotated about y-axis for scanning objects. Based on Eq. (9), the rotation angle θ_y is used to determine the normal vector from the laser projector frame to the camera frame as follows:

$$^{C}\boldsymbol{n} = {}^{C}_{L}\boldsymbol{R}_y {}^{L}\boldsymbol{n} = \begin{bmatrix} \cos\theta_y \\ 0 \\ -\sin\theta_y \end{bmatrix} \tag{11}$$

One can rewrite Eq. (11) as follows:

$$\cos\theta_y x - \sin\theta_y z -^{C} \boldsymbol{n} \cdot^{C} \boldsymbol{p}_{\mathrm{LORG}} = 0 \tag{12}$$

When the laser plane is projected to an object, features will be generated and captured in an image. Then, the equation of a line $l(s)$ can be determined by using the optical center of the camera and a feature point at $\boldsymbol{r} = (u, v)$ in the image frame as follows:

$$l(s) = \begin{cases} x = s \cdot u \\ y = s \cdot v \\ z = s \cdot f \end{cases} \tag{13}$$

The line in Eq. (13) and the plane in Eq. (12) intersect at a point on the surface of the object. To compute this 3-D point in the aid of Eq. (13), Eq. (12) can be rewritten as

$$\cos\theta_y(su) - \sin\theta_y(sf) -^{C} \boldsymbol{n} \cdot^{C} \boldsymbol{p}_{\mathrm{LORG}} = 0. \tag{14}$$

Thus, the parameter s can be uniquely determined to get the 3-D position $\boldsymbol{r}$ of the feature.

3.2 Calibration of active laser projection

Before executing 3-D reconstruction, the translation vector $\begin{bmatrix} p_x & p_y & p_z \end{bmatrix}^T$ from the camera to the laser projector must be calibrated. The component p_y along the y-axis is assumed as zero because the optical center of the laser projector is in the x-z plane of the camera frame. The rotations about the x-axis and z-axis of the laser projector are both assumed as zero, and only the rotation about the y-axis is allowed for the purpose of scanning objects in a pile. A model plane with a checkerboard pattern is placed in the workspace. By using the model plane and available geometric relationships, the values of the translation vector can be determined. Before performing the proposed calibration procedure, the camera must be calibrated in advance to obtain the intrinsic and distortion parameters. Table 1 shows the proposed calibration procedure.

Table 1 Calibration procedure for the pose of the laser line projector

– Place a model plane in the workspace.

– for ($i = 1;\ i \leq n; i + 1$)
{

Move the camera so that a corner point on the model plane coincides the principal point of the image.

Rotate the laser line projector about its y-axis until the laser line in the image passes through the principal point of the image frame.

if($i = 1$) {

Determine the distance d_1 between the camera and the model plane along the z-axis of the camera frame.
The rotation angle θ_1 is recorded and it must conform to

$$p_x \tan\theta_1 = p_z + d_1. \tag{18}$$

}
else {

Determine the variation d_i of the distance between the camera and the model plane along the z-axis of the camera frame.
The rotation angle θ_i is recorded and it must conform to

$$p_x \tan\theta_i = p_z + d_1 + d_i. \tag{19}$$

}
Change the position of the camera along the z-axis.
}

– Determine the value p_x by (19).
– Determine the value p_z by p_x and (19).

According to Table 1, when the model plane is captured in an image, the distance between the camera to the model plane can be determined by the known pattern as follows:

$$\lambda {}^{I}\boldsymbol{p} = \boldsymbol{K}\,{}^{C}_{N}\boldsymbol{T}\,{}^{N}\boldsymbol{p} \tag{15}$$

where λ is an arbitrary scale factor, ${}^{I}\boldsymbol{p}$ denotes a point in the image plane, $\boldsymbol{K}$ denotes the intrinsic matrix of the camera, ${}^{C}_{N}\boldsymbol{T}$ denotes the transformation matrix from the model plane frame $\{N\}$ to the camera frame $\{C\}$, and ${}^{D}\boldsymbol{p}$ denotes the corresponding 3-D point in the model plane frame $\{N\}$. Then, the laser line projector is rotated about the y-axis until the laser line in the image passes through the principal point of the image frame. At this stage, the rotation angle must conform to Eq. (18). Figure 5 shows the configuration of the calibration. In the next step, the camera moves along z-axis to change the distance to the model plane and the laser line projector rotates again until the laser line in the image passes through the principal point of the image frame. Equation (18) can be rewritten as Eq. (19). When the camera moves n times, the Eq. (19) can be organized as follows:

$$\begin{bmatrix} \tan\theta_1 \\ \tan\theta_2 \\ \vdots \\ \tan\theta_n \end{bmatrix} p_x = \begin{bmatrix} p_z + d_1 \\ p_z + d_1 + d_2 \\ \vdots \\ p_z + d_1 + d_n \end{bmatrix} \tag{16}$$

Moreover, Eq. (16) can be rewritten by subtracting Eq. (18) from Eq. (19) as follows:

$$\begin{bmatrix} \tan\theta_2 - \tan\theta_1 \\ \tan\theta_3 - \tan\theta_1 \\ \vdots \\ \tan\theta_n - \tan\theta_1 \end{bmatrix} p_x = \begin{bmatrix} d_2 \\ d_3 \\ \vdots \\ d_n \end{bmatrix}. \tag{17}$$

Then, the parameter p_x can be determined by solving Eq. (17). After solving p_x, the parameter p_z can be determined by using Eqs. (18) and (19).

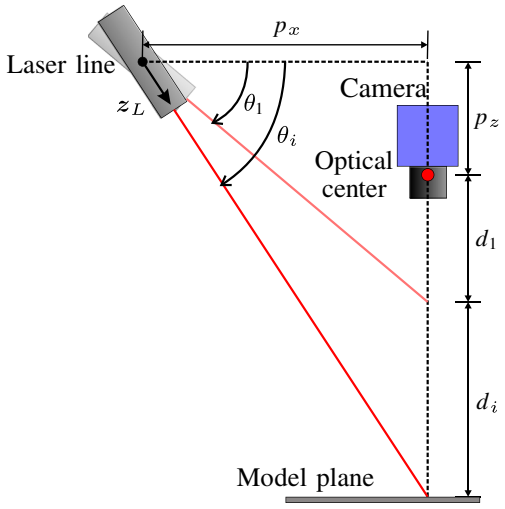

Fig. 5 The diagram of calibration

3.3 Point cloud segmentation

When the system reconstructs the point cloud of a pile of objects, the measured point cloud includes many objects. For the purpose of estimating the pose of a single object to be picked up, segmentation is an important step to get the point cloud of such an object. Neighboring point labeling is used to separate the point cloud of the top object. Based on gaps between different objects in a bin, the distance between neighboring points from different objects is farther than those from the same object. Table 2 shows the process. When the point cloud is obtained, the top point will be selected as the starting point from the highest object. Then, the system searches neighboring points by computing distances between points. Selected points are labeled and used to search for other neighboring points. The threshold value d^* is used to separate point clouds of neighboring objects. If neighboring objects are closer, d^* can be adjusted smaller to correctly identify points for each neighboring part. After all neighboring points are labeled, the system can identify a point cloud for a single object. If labeled points are considerably fewer, those points will be removed and then the system selects a new point to search neighboring points again.

Table 2 Point cloud segmentation

- Input the data point cloud.
- Search the top point of the point cloud and save it to a queue.
- Label the top point to avoid being assigned to the queue again.
- while (the number of points in the queue $\neq 0$)
  {

    Take out a point g from the queue.

    Let g_c be the center and search all neighboring points with a pre-determined distance except labeled points.
    for($i = 1;\ i \leq n; i + 1$) {

      if(g_i is labeled)
        continue;
      Determine the distance d between g_c and g_i.
      if($d < d^*$)
        Input the point g_i to the queue and label it.
    }
  }
- Save all labeled points as the point cloud of the top object.

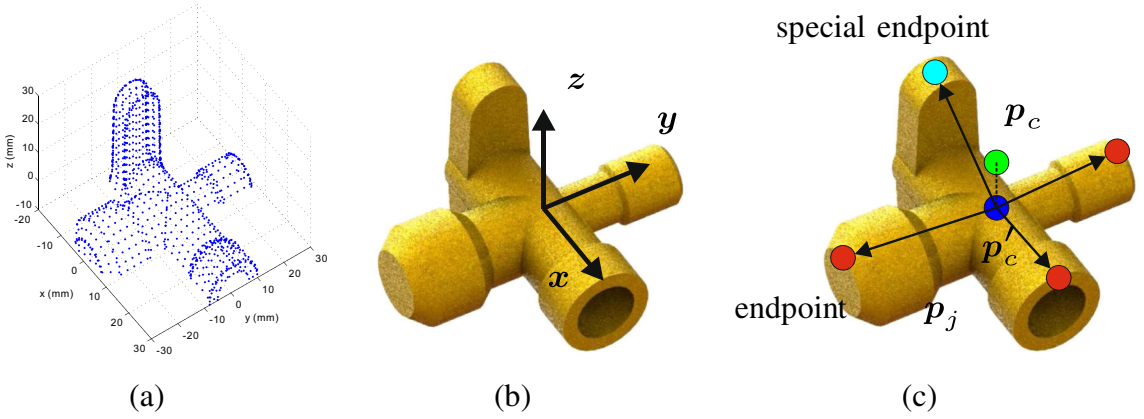

Fig. 6 **a–c** The model point cloud and design of object

4 Pose estimation

In order to estimate the pose of an object, the ICP algorithm can be employed to determine the transformation from model point cloud frame $\{M\}$ to data point cloud frame $\{D\}$. The model point cloud is generated by software based on the original design of an object. According to the design data, one computes the 3-D points equally distributed on the object surface and the number of points can be set appropriately by the density parameter. Figure 6a shows the model point cloud. The pose of the model point cloud is known a priori, so the pose of an object can be determined by the transformation from the model point cloud. It is indeed a practical problem if the geometry of the object is complex and the deviation of the data point cloud from the model point cloud is large; the result of point cloud matching may fail. To solve this problem, the CCP approach is proposed to roughly estimate the pose of the data point cloud and then the ICP algorithm is employed to precisely matching two point clouds.

4.1 Feature-geometric computed closer point

Feature-geometric CCP approach is proposed to approximately estimate the transformation between two point clouds based on the geometry of a plumbing part. By analyzing the geometry, an appropriate estimation strategy can be formulated and it executes quickly and efficiently. The shape of the plumbing part includes three cylindrical and one elliptical geometric features. The x-axis and y-axis are attached along the cylindrical features as shown in Fig. 6b. Because of the symmetry, only half of the object is considered. As with the estimation of translation from the model point cloud to the data point cloud ${}^{M}p_{D}$, the centers of two point clouds are determined by averaging all points, respectively. For estimating the difference in orientation between two point clouds, the cylindrical features can be considered. In order to detect those characteristics, the following steps need to be performed accordingly.

1. Let X be a data point cloud set with n points and $X = \{\boldsymbol{p}_i\}$ for $i = 1, \cdots, n$. Determine the center of mass of the data point cloud by averaging all points.

$$\boldsymbol{p}_{\mathrm{c}} = \frac{1}{n}\sum_{i=1}^{n} \boldsymbol{p}_i. \tag{20}$$

2. Set $\boldsymbol{p}_{\mathrm{c}}$ as the center point and select the points where the distance between the point and $\boldsymbol{p}_{\mathrm{c}}$ is within a range s as follows:

$$\| \boldsymbol{p}_i - \boldsymbol{p}_{\mathrm{c}} \| \leq s \tag{21}$$

   By averaging these points, a new center point $\boldsymbol{p}'_{\mathrm{c}}$ can be determined. This center point is closer to the surface of the object than $\boldsymbol{p}_{\mathrm{c}}$.
3. Identify endpoints by selecting the farthest points along four different directions. Then, compute the vectors from $\boldsymbol{p}'_{\mathrm{c}}$ to all endpoints and normalize those vectors as follows:

$$\boldsymbol{h}_j = \frac{\boldsymbol{p}_j - \boldsymbol{p}'_{\mathrm{c}}}{\| \boldsymbol{p}_j - \boldsymbol{p}'_{\mathrm{c}} \|}, \tag{22}$$

Table 3 The simulation cases

Case	Points		Initial pose of data point cloud					
			Position (mm)			Rotation (deg)		
	n_m	n_d	x	y	z	θ_x	θ_y	θ_z
1	300	100	100	100	100	10	0	0
2	300	100	200	200	200	77	83	51
3	300	300	0	0	0	10	0	0
4	300	300	0	0	0	−10	0	0
5	300	300	100	100	100	10	0	0
6	300	300	200	200	200	77	83	51

where $\boldsymbol{p}_j$ denotes the endpoint for $j = 1, \cdots, 4$.

4. Average four endpoints $\boldsymbol{p}_j$ to determine the mass of center of endpoints, $\boldsymbol{p}_e$, and determine the unit vector $\boldsymbol{v}$ along the direction from $\boldsymbol{p}'_c$ to $\boldsymbol{p}_e$:

$$\boldsymbol{v} = \frac{\overrightarrow{\boldsymbol{p}'_c \boldsymbol{p}_e}}{\| \overrightarrow{\boldsymbol{p}'_c \boldsymbol{p}_e} \|}. \tag{23}$$

5. Project the vectors of step 3 to $\boldsymbol{v}$,

$$\frac{\boldsymbol{h}_j \cdot \boldsymbol{v}}{\| \boldsymbol{v} \|}, \tag{24}$$

and then two endpoints corresponding to two minimum projection values can be assigned as the approximate endpoints of cylindrical features. To determine the special endpoint from remaining points, set $\boldsymbol{p}'_c$ as center of circle and a length as radius and determine the equation of a plane by using the points in this range. The point with the farthest distance from this plane is identified as the special endpoint. The other three endpoints are members of three groups A, B, and C, respectively.

6. Determine the lines connecting the center point $\boldsymbol{p}'_c$ to endpoints except special endpoint, respectively. Next, set a threshold value τ to classify points to the corresponding group. Every point $\boldsymbol{p}_i$ is included in a group if the distance between the point and the endpoint of this group is less than τ and the distance from this point to the line of the group is the shortest one. If a point is classified to group A, the following conditions must be satisfied:

$$\| \boldsymbol{p}_i - \boldsymbol{p}_A \| < \tau, \tag{25}$$

$$\min(\lambda_{i,A}, \lambda_{i,B}, \lambda_{i,C}) = \lambda_{i,A}, \tag{26}$$

where $\lambda_{i,A}$ denotes the distance between the point $\boldsymbol{p}_i$ and the line of group A

$$\lambda_{i,A} = \| \overrightarrow{\boldsymbol{p}_i \boldsymbol{p}_A} - \frac{\overrightarrow{\boldsymbol{p}_i \boldsymbol{p}_A} \cdot \overrightarrow{\boldsymbol{p}'_c \boldsymbol{p}_A}}{\| \overrightarrow{\boldsymbol{p}'_c \boldsymbol{p}_A} \|^2} \overrightarrow{\boldsymbol{p}'_c \boldsymbol{p}_A} \| . \tag{27}$$

In this step, points near the center point $\boldsymbol{p}'_c$ are not classified to any group.

7. After classification, determine the average point of each group. Then, determine an unit vector along the direction from $\boldsymbol{p}'_c$ to each average group point.
8. Compute inner product for each two vectors described in step 7. The vector with both smallest inner products with the other two vectors is assigned as the x-axis $\boldsymbol{x}_D$. The vector of y-axis, $\boldsymbol{y}_D$, can be identified from the remaining two vectors that corresponds to fewer group points with shorter distance to its group center and orthogonal to $\boldsymbol{x}_D$. According to the coordinate vectors determined from the data point cloud, one can determine the orientation of the object as follows:

$$\bar{D}_D \boldsymbol{R} = \left[\boldsymbol{x}_D \ \boldsymbol{y}_D \ \boldsymbol{z}_D \right], \tag{28}$$

where $\boldsymbol{z}_D$ denotes the vector of z-axis determined by outer product of $\boldsymbol{x}_D$ and $\boldsymbol{y}_D$. The transformation from

Table 4 The simulation results

Case	Approach	Pose estimation error						Execution time (s)
		Position (mm)			Rotation (deg)			
		x	y	z	θ_x	θ_y	θ_z	
1	ICP	2.89	0.58	6.78	142.69	−66.39	−155.21	0.58
	CCP + ICP	−1.52	1.6	−0.99	0.84	0.31	0.2	0.61
2	ICP	1.15	−8.18	3.88	−214.61	−39.01	69.89	1.01
	CCP + ICP	0.75	1.36	1.02	4.99	0.53	4.56	0.40
3	ICP	0.06	0.33	0.19	0.13	0.36	0.1	1.60
	CCP + ICP	0.51	0.21	0.15	0.01	0.46	−0.13	2.05
4	ICP	0.08	0.3	0.06	0.1	0.43	−0.1	0.94
	CCP + ICP	0.51	0.21	0.15	0.01	0.46	−0.13	2.46
5	ICP	−4.14	0.23	6.16	113.26	59.88	15	2.07
	CCP + ICP	−1.45	1.69	−0.41	0.04	0.57	0.1	1.78
6	ICP	0.86	6.15	−4.97	134.19	−93.45	−113.3	4.36
	CCP + ICP	−0.05	1.55	1.6	−0.63	0.01	−0.6	1.46

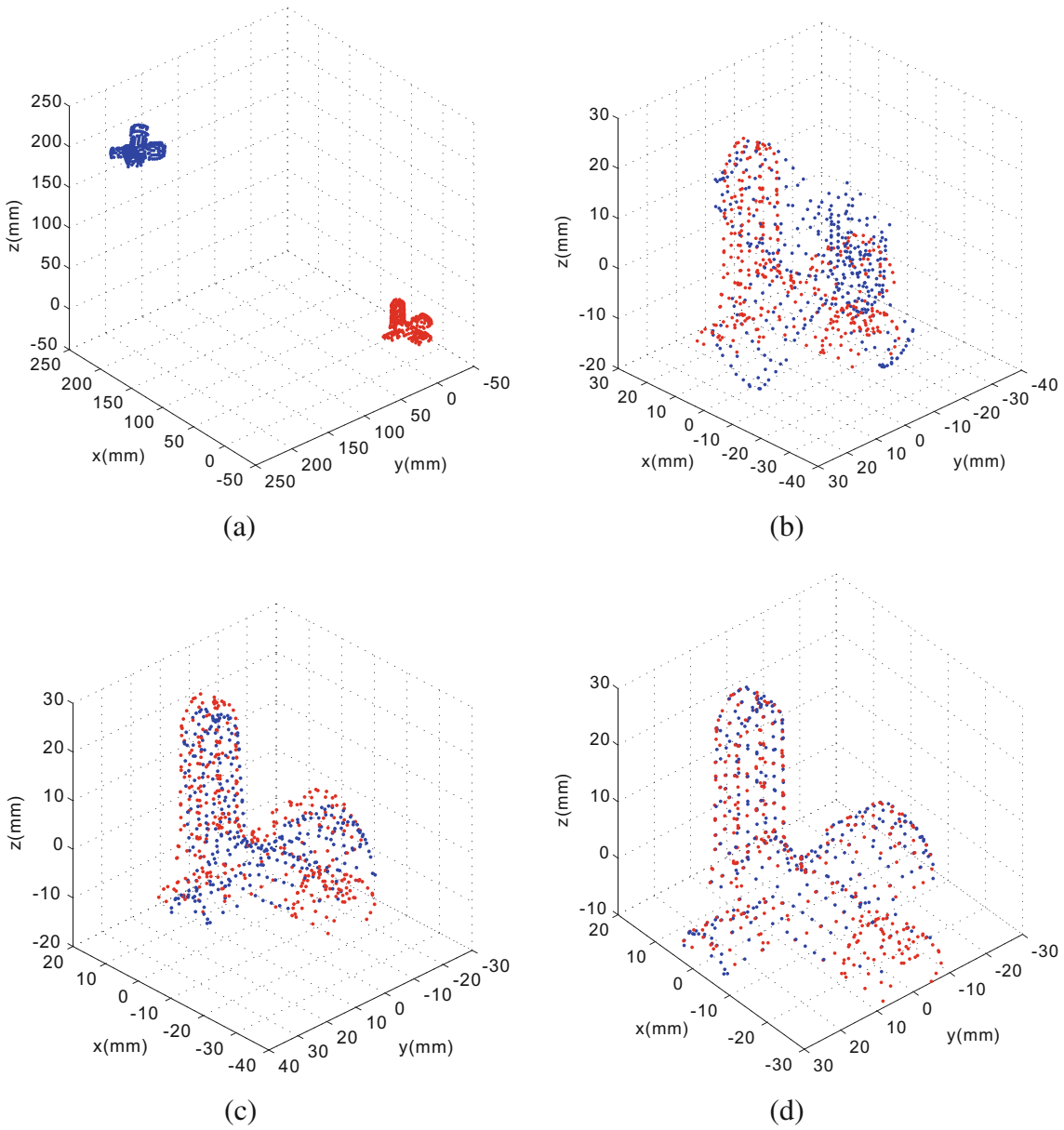

Fig. 7 **a–d** The simulation results of case 6

$\{\bar{D}\}$ to $\{D\}$ can be determined by ${}^{\bar{D}}_{D}\boldsymbol{R}$ and ${}^{\bar{D}}\boldsymbol{p}_D$ as follows:

$$ {}^{\bar{D}}_{D}\boldsymbol{T} = \begin{bmatrix} {}^{\bar{D}}_{D}\boldsymbol{R} & {}^{\bar{D}}\boldsymbol{p}_D \\ 0_{1\times 3} & 1 \end{bmatrix} \tag{29} $$

After performing CCP approach, the data point cloud is transformed by ${}^{\bar{D}}_{D}\boldsymbol{T}$. The pose of transformed data point cloud will be closer to model point cloud.

Table 5 The allowed translation of objects

	ICP	Computed closer point + ICP
1 axis	Small	Large
3 axes	Small	Large

4.2 Point cloud matching

By using feature-geometric CCP approach, the pose of an object can be determined roughly and one can determine the transformation matrix ${}^{\bar{D}}_{D}\boldsymbol{T}$ based on the pose attached with the closer object frame $\{\bar{D}\}$. Then, the data point cloud will be moved to new pose according to ${}^{\bar{D}}_{D}\boldsymbol{T}$, and the pose is

Table 6 The allowed rotation of objects

	ICP (deg)	Computed closer point + ICP (deg)
1 axis	±30	±180
3 axes	±15	±180

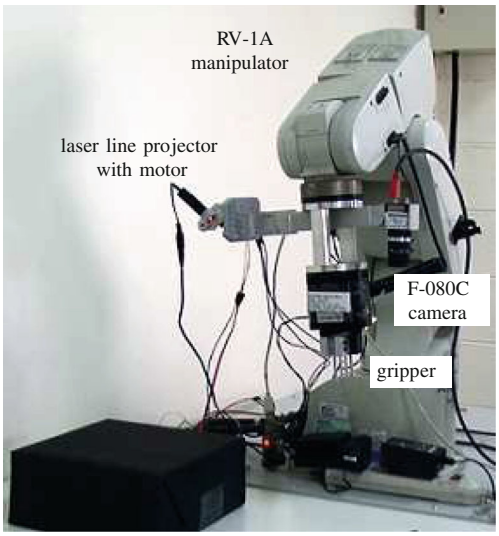

Fig. 8 The configuration of experiment

approaching to the model point cloud. The system employs the ICP algorithm to determine the transformation matrix from the model point cloud to the data point cloud, ${}^{M}_{D}\boldsymbol{T}_{\mathrm{ICP}}$, after performing CCP approach. After the iterations of the ICP computation, the accurate pose of data point cloud thus can be determined from the transformation matrix by Eq. (6). The transformation matrix from base frame $\{B\}$ to model point cloud frame $\{M\}$, ${}^{B}_{M}\boldsymbol{T}$, is known a priori and the pose of the object in the base frame can be determined by Eq. (3). To determine a command for driving the manipulator to a pose before further grasping, the desired transformation ${}^{G}_{D}\boldsymbol{T}$ between the gripper frame $\{G\}$ and the object frame $\{D\}$ must be pre-determined. Based on the transformation ${}^{B}_{D}\boldsymbol{T}$ in Eq. (3), the desired transformation between the base frame and the gripper frame is determined as follows:

$$ {}^{B}_{G}\boldsymbol{T} = {}^{B}_{D}\boldsymbol{T}\,{}^{G}_{D}\boldsymbol{T}^{-1} = \begin{bmatrix} {}^{B}_{G}\boldsymbol{R}(\boldsymbol{\theta}_G) & {}^{B}\boldsymbol{p}_G \\ \boldsymbol{0}_{1\times 3} & 1 \end{bmatrix} \tag{30} $$

Then, the pose command can be computed based on $\boldsymbol{\theta}_G$ and ${}^{B}\boldsymbol{p}_G$.

To speed up iterations of the ICP algorithm, KD tree is also be used to improve the performance of the closest point searching [9]. KD tree is effective to reduce points for searching. If the number of points in the model point cloud is large in nature, the computation will be much more efficient for iterations of the ICP algorithm once KD tree is employed.

5 Simulation and experiments

5.1 Simulations

The proposed approach has been simulated with a predetermined model point cloud. Half of the model point cloud was considered because of its symmetry. A data point cloud is generated by using model point cloud with some variations. Table 3 shows six cases of the simulations. The number of data points in the model point cloud, n_m, is 300 and one of the data point cloud, n_d, is 100 or 300. The initial pose denotes the pose of the data point cloud before matching process. There are several different poses of the data point cloud to test the performance of the ICP algorithm with and without CCP. Table 4 shows the results of simulations, where the ICP algorithm and CCP then ICP

(a) (b)

Fig. 9 **a**, **b** The original image of the targets and the image after image processing

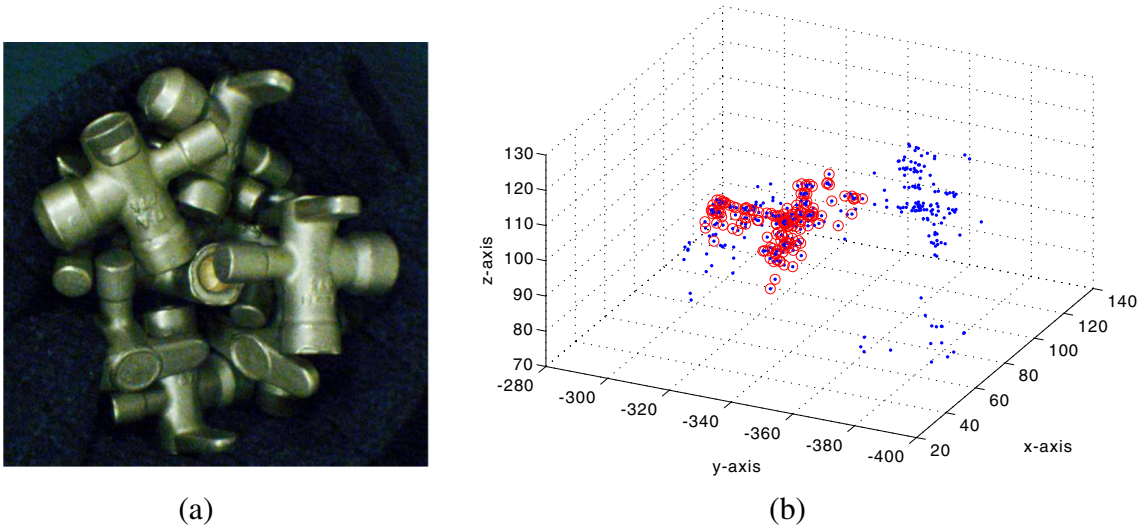

(a) (b)

Fig. 10 **a**, **b** The actual image and reconstructed point cloud

are both tested for point cloud matching. Estimation error denotes the pose error of the data point cloud after point cloud matching. According to the simulations, it shows that if deviation between two point clouds is small, the ICP can succeed after appropriate number of iterations. For large deviation between two point clouds, the CCP must be employed to roughly estimate the pose of data point cloud first and then iterations of ICP could converge successfully. Using CCP can decrease execution time because the number of iteration is reduced. For the execution time of the proposed approach, the computation of the ICP algorithm spends most of the time for iterations. If the efficiency of the ICP computation can be further improved, the execution time of the proposed approach can be much more reduced. Figure 7 shows the simulations of case 6 that the pose of data point cloud is wrong by using the ICP algorithm because of large deviation between two point clouds. Figure 7c shows that the pose of data point cloud after CCP is similar to that of model point cloud. So, it successfully matched two point clouds. According to the results of the simulations, the performance of the ICP algorithm and the proposed CCP then ICP algorithm can be generalized as shown in Tables 5 and 6. Because the CCP computes based on the geometry of a plumbing part, the approach is able to apply to any pose of the data point cloud.

5.2 Experiments

To implement the proposed system, a Mitsubishi RV-1A 6-DOF robotic manipulator with gripper, an AVT Guppy F-080C camera, and a laser line projector with a DC motor are employed in the system. A pair of designed jaws is attached to the gripper. The system is shown in Fig. 8. The resolution of camera is 1032 × 778 and the frame rate for image processing is 15 fps. When the system starts, the motor will be driven to rotate continuously with 1° resolution until the maximum degree and the camera will capture the image continuously at the same time. When the image is captured, the image processing is executed to identify the features from the laser line projection. The color space is transformed from RGB to YCrCb. By setting appropriate threshold values, the image can be filtered to binary image that red denotes the rough range of features and white denotes the other region. Then, one can use the thinning algorithm to locate accurate features. Figure 9 shows the result of the image processing. To reduce the execution time, data sampling was employed in reconstruction step to adjust the intensity of points. The experimental result is shown in Fig. 10. The system reconstructed a point cloud for a pile of plumbing parts and detected the data point cloud of the top plumbing part denoted by red circle in Fig. 10b. After the pose estimation of the plumbing part, the system computed

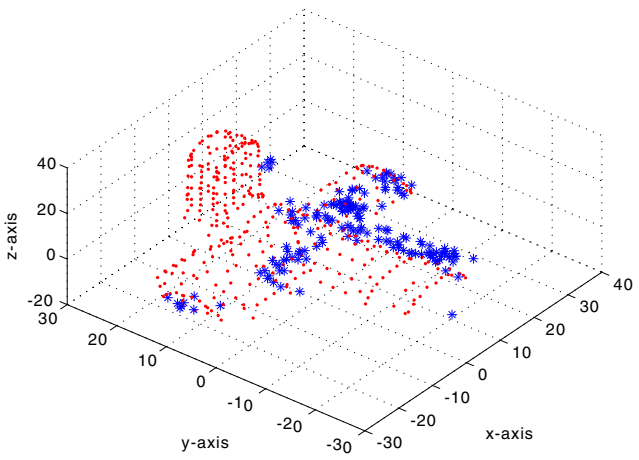

Fig. 11 The matched point cloud shown in the model point cloud

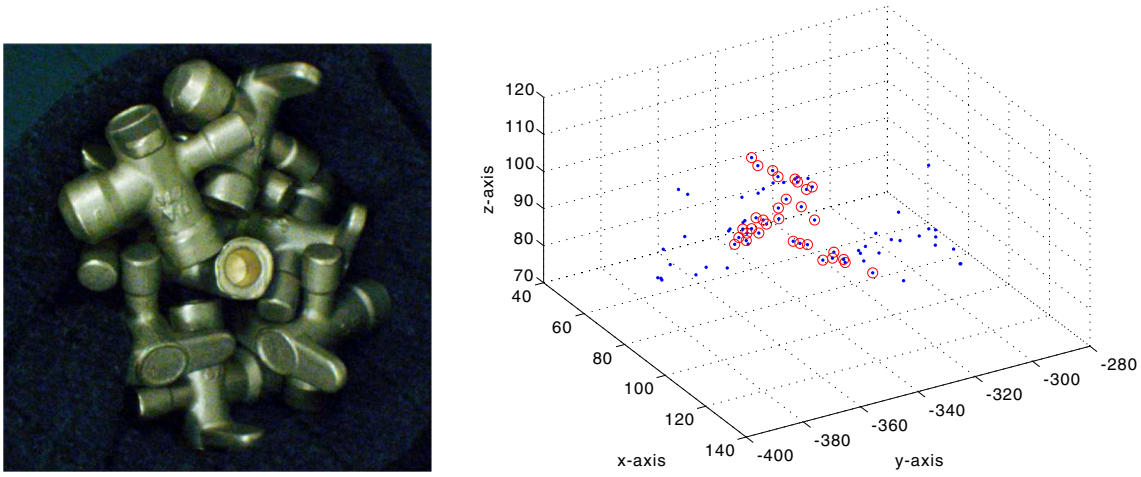

Fig. 12 **a**, **b** The actual image and reconstructed point cloud

the transformation matrix from base frame to object frame as the following:

$$ {}^{B}_{D}\boldsymbol{T}_1 = \begin{bmatrix} -0.2153 & 0.9630 & -0.1624 & 67.0372 \\ 0.9755 & 0.2198 & 0.0103 & -355.346 \\ 0.0456 & -0.1562 & -0.9867 & 153.6095 \\ 0 & 0 & 0 & 1 \end{bmatrix}. \quad (31) $$

The result of point cloud matching is shown in Fig. 11, where the red point denotes the model point cloud and the blue star denotes the data point cloud. According to the transformation matrix, the command can be determined to drive the manipulator to grip the target. Figures 12 and 13 show another experimental result. The transformation from base frame to object frame is

$$ {}^{B}_{D}\boldsymbol{T}_2 = \begin{bmatrix} -0.718 & 0.6929 & 0.0664 & 100.939 \\ 0.6736 & 0.7157 & -0.1845 & -346.657 \\ -0.1754 & -0.0878 & -0.9806 & 143.9666 \\ 0 & 0 & 0 & 1 \end{bmatrix}. \quad (32) $$

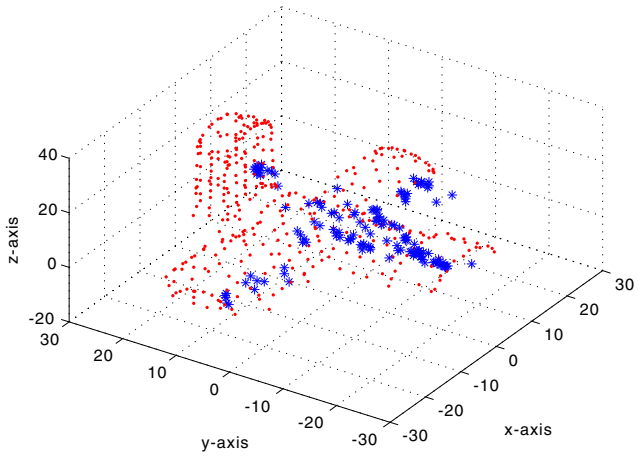

Fig. 13 The matched point cloud shown in the model point cloud

It shows that the pose of the object was effectively estimated because the model point cloud and data point cloud are matched successfully.

The proposed CCP then ICP approach has been validated in experiments. Although objects are stacked in a pile, the proposed approach can effectively observe and pick up the top object. When some portion of the data point cloud are not available, the proposed approach might still work successfully if the major features are maintained. Moreover, by performing the approach repeatedly, it appears that potential applications in production line can be expected. To compare with the existing system from Fanuc [7], the characteristics are shown in Table 7. Fanuc bin-picking robot employs a projector to project coded structured light and uses two cameras to capture images for the purpose of identifying object poses. The sensor configuration in our proposed system is eye-in-hand rather than eye-to-hand. Thus, it appears to be an advantage in flexibility that the system is able to reconstruct objects at different directions. 3-D data is used in both systems that is useful to identify objects and then determine the poses.

Table 7 The comparison with Fanuc bin-picking robot

	Proposed system	Fanuc system
Sensor	Active laser projector with a camera	Projector with two cameras
Sensor structure	Eye-in-hand	Eye-to-hand
Structured light	A straight line	Coded gray structured light
Manipulator	6-DOF manipulator	6-DOF manipulator

6 Conclusion

The proposed system employs an eye-in-hand camera with active laser projection to reconstruct the point cloud of a pile of plumbing parts. After employing point cloud segmentation, the point cloud of the top object can be identified. To determine the pose of object successfully, the feature-geometric CCP is proposed to roughly estimate the pose of object and then the ICP algorithm is employed to precisely match the data and model point clouds. Thus, the pose of the object can be determined in order for the manipulator to grasp the object correctly. The experiments have been successfully validated since the system can correctly identify and then grasp the object. This system can be applied in industrial automation to improve the performance of existing production line.

Acknowledgments This research was supported by the Industrial Technology Research Institute, Taiwan, R.O.C. under grant C301AA4110-FY102.

References

1. Bellandi P, Docchio F, Sansoni G (2013) Roboscan: a combined 2D and 3D vision system for improved speed and flexibility in pick-and-place operation. Int J Adv Manuf Technol 69(5–8):1873-1886. doi:10.1007/s00170-013-5138-z
2. Besl P, McKay H (1992) A method for registration of 3-D shapes. IEEE Trans Pattern Anal Mach Intell 14(2):239-256. doi:10.1109/34.121791
3. Chen Y, Dong F (2013) Robot machining: recent development and future research issue. Int J Adv Manuf Technol 66(9–12):1489–1497
4. Cheng JT, Wang CJ, Zhao C, Mo JH (2007) Design of a servo motion system and an image sampling and processing system on a 3D laser scanner. Int J Adv Manuf Technol 33(11–12):1143-1148. doi:10.1007/s00170-006-0555-x
5. Chetverikov D, Stepanov D, Krsek P (2005) Robust Euclidean alignment of 3D point sets: the trimmed iterative closest point algorithm. Image Vis Comput 23(3):299–309
6. Du S, Zheng N, Ying S, Liu J (2010) Affine iterative closest point algorithm for point set registration. Pattern Recogn Lett 31(9):791–799
7. Fanuc Ltd (2015). http://www.fanuc.co.jp
8. Ferreira M, Moreira AP, Neto P (2012) A low-cost laser scanning solution for flexible robotic cells: spray coating. Int J Adv Manuf Technol 58(9–12):1031-1041. doi:10.1007/s00170-011-3452-x
9. Greenspan M, Yurick M (2003) Approximate K-D tree search for efficient ICP. In: Fourth International Conference on 3-D Digital Imaging and Modeling, 2003, 3DIM 2003, pp 442-448. doi:10.1109/IM.2003.1240280
10. Griffin PM, Narasimhan LS, Yee SR (1992) Generation of uniquely encoded light patterns for range data acquisition. Pattern Recogn Lett 25(6):609–616
11. Gushov V, Solodkin Y (1991) Automatic processing of fringe patterns in integer interferometers. Opt Lasers Eng 14(4–5):311–324. doi:10.1016/0143-8166(91)90055-X. http://www.sciencedirect.com/science/article/pii/014381669190055X
12. Kristensen S, Estable S, Kossow M, Brosel R (2001) Bin-picking with a solid state range camera. Robot Auton Syst 35(3–4):143-151. doi:10.1016/S0921-8890(01)00123-3. Seventh Symposium on Intelligent Robotic Systems - SIRS1699
13. Lin AC, Hui-Chin C (2011) Automatic 3D measuring system for optical scanning of axial fan blades. Int J Adv Manuf Technol 57(5–8):701–717. doi:10.1007/s00170-011-3329-z
14. Li F, Longstaff AP, Fletcher S, Myers A (2014) Rapid and accurate reverse engineering of geometry based on a multi-sensor system. Int J Adv Manuf Technol 74(1-4):369–382
15. Milroy M, Weir D, Bradley C, Vickers G (1996) Reverse engineering employing a 3D laser scanner: a case study. Int J Adv Manuf Technol 12(2):111-121. doi:10.1007/BF01178951
16. Pochylym A, Kubela T, Kozak M, Cihak P (2010) Robotic vision for bin-picking applications of various objects. In: Robotics (ISR), 2010 41st International Symposium on and 2010 6th German Conference on Robotics (ROBOTIK), pp pp 1-5
17. Posdamer J, Altschuler M (1982) Surface measurement by space-encoded projected beam systems. Comput Graphics Image Process 18(1):1–17
18. Rodrigues J, Kim JS, Furukawa M, Xavier J, Aguiar P, Kanade T (2012) 6D pose estimation of textureless shiny objects using random ferns for bin-picking. In: Intelligent Robots and Systems (IROS), 2012 IEEE/RSJ International Conference on, pp 3334–3341. doi:10.1109/IROS.2012.6385680
19. Sansoni G, Bellandi P, Leoni F, Docchio F (2014) Optoranger: A 3D pattern matching method for bin picking applications. Opt Lasers Eng 54(0):222–231. doi:10.1016/j.optlaseng.2013.07.014. http://www.sciencedirect.com/science/article/pii/S0143816613002303
20. Srinivasan V, Liu HC, Halioua M (1985) Automated phase-measuring profilometry: a phase mapping approach. Appl Opt 24(2):185–188
21. Tao J, Juntong X, Junqi Y (2006) An accurate three-dimensional scanning system with a new phase error compensation method. Int J Adv Manuf Technol 29(11–12):1178–1185. doi:10.1007/s00170-005-0015-z
22. Turley GA, Kiraci E, Olifent A, Attridge A, Tiwari MK, Williams MA (2014) Evaluation of a multi-sensor horizontal dual arm coordinate measuring machine for automotive dimensional inspection. Int J Adv Manuf Technol 72(9-12):1665–1675
23. Xu J, Pu S, Zeng G, Zha H (2012) 3D pose estimation for bin-picking task using convex hull. In: 2012 International Conference on Mechatronics and Automation (ICMA), pp 1381-1385. doi:10.1109/ICMA.2012.6284338
24. Ying S, Peng J, Du S, Qiao H (2009) A scale stretch method based on ICP for 3D data registration. IEEE Trans Autom Sci Eng 6(3):559-565. doi:10.1109/TASE.2009.2021337
25. Zhang YC, Han JX, Fu XB, Lin HB (2014) An online measurement method based on line laser scanning for large forgings. Int J Adv Manuf Technol 70(1–4):439–448. doi:10.1007/s00170-013-5240-2